ACS OMEGA

http://pubs.acs.org/journal/acsodf

Article

Toward a Mechanically Rechargeable Solid Fuel Flow Battery Based on Earth-Abundant Materials

Alexis M. Fenton, Jr.,[¶] Yasser Ashraf Gandomi,[¶] Christopher T. Mallia, Bertrand J. Neyhouse, M. Aba Kpeglo, William E. Exson, Charles Tai-Chieh Wan, and Fikile R. Brushett*

Cite This: *ACS Omega* 2022, 7, 40540−40547

Read Online

ACCESS | Metrics & More | Article Recommendations | Supporting Information

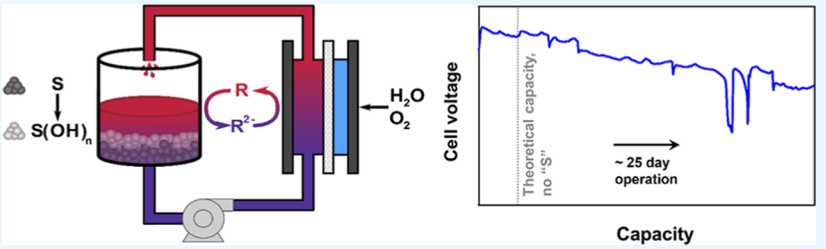

ABSTRACT: Metal−air batteries are a promising energy storage solution, but material limitations (e.g., metal passivation and low active material utilization) have stymied their adoption. We investigate a solid fuel flow battery (SFFB) architecture that combines the energy density of metal−air batteries with the modularity of redox flow batteries. Specifically, a metallic solid electrochemical fuel (SEF) is spatially separated from the anodic current collector, a dissolved redox mediator (RM) shuttles charges between the two, and an oxygen reduction cathode completes the circuit. This modification decouples power and energy system components while enabling mechanical recharging and mitigating the effects of nonuniform metal oxidation. We conduct an exploratory study showing that metallic SEFs can chemically reduce organic RMs repeatedly. We subsequently operate a proof-of-concept SFFB cell for *ca.* 25 days as an initial demonstration of technical feasibility. Overall, this work illustrates the potential of this storage concept and highlights scientific and engineering pathways to improvement.

INTRODUCTION

Electrochemical energy storage is anticipated to be an important component of a sustainable energy economy, and the continued development of rechargeable battery technologies is key to global decarbonization efforts.[1,2] While numerous rechargeable batteries have been developed, lithium-ion (Li-ion) batteries represent the current state of the art due to their favorable combination of power density, efficiency, and cycle life. However, the energy density, cost, and scale requirements of emerging applications (e.g., heavy-duty transportation and long-duration storage) challenge current Li-ion battery technologies, motivating research and development into a diverse array of redox chemistries and system formats that may better suit current and future societal needs.

Metal−air batteries have attracted considerable attention over the years due in part to the high charge-storage capacity of metallic negative electrodes—along with the low cost and high terrestrial abundance of oxygen (O_2)—which, taken together, offer a pathway to inexpensive and energy dense storage.[3−5] While these batteries have found success as primary (non-rechargeable) applications (e.g., hearing aids), deployment of rechargeable batteries at large scales has generally been hampered by a combination of low active material utilization, limited cycle life, and poor roundtrip energy efficiency.[3] Herein, we explore opportunities to enable more versatile operation by mitigating some of these limitations through an alternative cell design: the solid fuel flow battery (SFFB). Specifically, instead of utilizing a conventional enclosed cell typical of most metal−air batteries, the SFFB adopts a hybrid architecture more akin to that of redox flow batteries (RFBs) and direct liquid fuel cells, where a metallic solid electrochemical fuel (SEF) is housed in an external tank spatially separated from the electrochemical reactor. A solubilized redox mediator (RM) transports charge between the SEF and the anodic current collector (Figure 1), and the cathodic O_2 reduction reaction (ORR) completes the electrical and ionic circuits *via* a gas diffusion electrode.

Such spatial decoupling eliminates the need to maintain electrical contact between the current collector and the metal, ostensibly reducing the detrimental effects of passivation and lowering the materials processing requirements. For example, by mechanically exchanging zinc in a modular fashion, the

Received: September 6, 2022
Accepted: September 23, 2022
Published: October 25, 2022

https://doi.org/10.1021/acsomega.2c05798
ACS Omega 2022, 7, 40540−40547

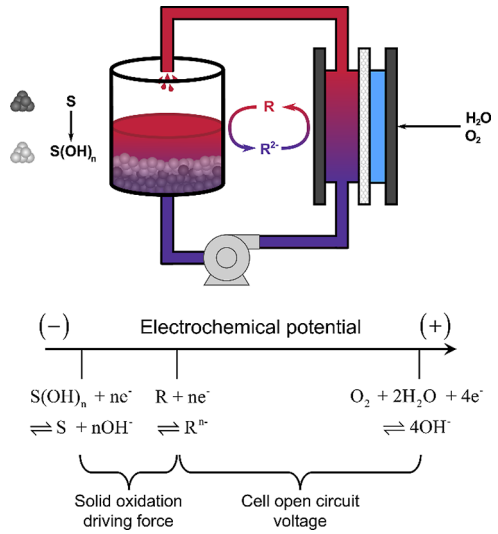

Figure 1. Schematic illustration of the SFFB. In the cathode, O_2 and water react to form hydroxyl ions, which cross the membrane to the anodic half-cell. There, the reduced RM "R^{2-}" is oxidized to R, which, along with the hydroxyl ions, are subsequently pumped to the storage tank, where the SEF ("S") oxidizes as it chemically reduces R to R^{2-}. The recharged R^{2-} is then pumped to the anode to be reoxidized. Below the diagram, the reactions are shown on an electrochemical potential schematic; relative potential spacings are for conceptual illustration and are not drawn to scale.

metal may necessitate less stringent specifications than are required for conventional immobile metal electrodes, increasing materials flexibility. In a similar manner, the overall energy capacity may scale volumetrically as, in principle, the entire metal surface can be accessed (i.e., less stringent electrode thickness constraints). Within the SFFB, charging is designed to be exclusively conducted by mechanical recharging *via* facile periodic SEF exchange (i.e., no electrochemical charging occurs);[6−8] this may simplify the recharging process—rather than replacing entire cells, only fuels need be exchanged (i.e., less inactive material replacement). Mechanical recharging may also potentially circumvent the challenges of metal electrodeposition at high rates and long durations. Further, this architecture may enable multiple different SEF−RM pairings to be used depending on the installation site, materials availability, or process economics. Overall, these benefits make the SFFB a promising energy storage concept with potentially increased versatility in material composition, modification, and maintenance.

In recent years, there have been several reports that describe electrochemical processes that use solubilized RMs to transfer charge between physically separated reactants and an electrode for the purpose of energy storage and conversion.[7−14] Wang *et al.* have pioneered rechargeable mediated flow batteries with solid active materials in external tanks *via* redox targeting—the process of selecting or engineering RMs by modulating their redox potential to favorably exchange electrons with a solid (insoluble) material.[9,10] Deng *et al.* have also demonstrated a fuel cell targeting biomass byproducts of pulp and paper processing using iron (Fe)-based mediators, while Stahl *et al.* have extensively studied mediated fuel cell architectures with both organic and inorganic redox chemistries.[11,12] Recent demonstrations by Perez-Antolin *et al.* and Zhang *et al.* have also shown that similar architectures (e.g., refillable primary batteries with semi-solid slurries, zinc−air flow batteries leveraging redox-mediated ORR) are promising.[7,8] Here, we leverage these previous research efforts to further explore the implementation of metallic SEFs into modified metal−air systems; we particularly focus on RM−SEF interactions in the storage tank (Figure 1). We first use *in situ* microelectrode voltammetry, post-mortem X-ray diffractometry, and post-mortem optical microscopy to assess the efficacy of RM−SEF pairings—identifying 2-hydroxynaphthoquinone (2-HNQ) and zinc (Zn) as a favorable combination. We then assemble a proof-of-concept cell and demonstrate galvanostatic operation over *ca.* 25 days, discharging *ca.* 30% of the Zn in the external tank. Overall, this work seeks to articulate foundational design principles and experimental methods for SFFBs and aims to inspire future studies that expand upon this demonstration and, more generally, modified metal−air systems.

RESULTS AND DISCUSSION

Materials Selection Criteria. The first criterion for successful operation of an SFFB is a suitable SEF and RM combination. As illustrated in Figure 1, there must be a sufficient thermodynamic driving force between the SEF and the RM to promote the chemical redox reaction, yet too great a driving force lowers the cell voltage and thus the accessible power and energy density. Parasitic side reactions (e.g., hydrogen evolution) must also be mitigated. We selected Zn and Fe as candidate SEFs and 2-HNQ and 2,6-dihydroxyanthraquinone (2,6-DHAQ) as candidate RMs. Fe and Zn are earth-abundant metals with extensive histories as anodes in aqueous metal−air battery literature, while 2-HNQ and 2,6-DHAQ have recently been demonstrated in aqueous organic RFBs.[6,15−17] Further, the 2,6-DHAQ/Zn pairing has already been successfully demonstrated to improve cell performance, though analytical studies (e.g., ultraviolet−visible photospectrometry, voltammetry) of this RM−SEF pairing were not specifically presented in the prior work.[7] To enable greater materials compatibility, reduce the propensity for hydrogen generation, and close the supporting ion balance, we investigated cell operation in an alkaline environment. We explored all four combinations of SEFs and RMs; only the results for the best-performing pair—Zn and 2-HNQ—are described in the main text, while those of other pairings are found in the Supporting Information. We note that these mediator-solid pairings only promote discharge reactions; mechanical recharging *via* zinc replacement may be faster compared to electrochemical methods, potentially making the SFFB an attractive option for off-grid applications.

In this system, the specific (electro)chemical (half-)reactions proposed to take place in the storage tank at the anode and the cathode are, respectively, detailed in eqs 1−3.

$$2Zn + 4OH^- \rightleftharpoons 2ZnO + 2H_2O + 4e^- \quad (1)$$

$$2\text{-}HNQ^- + 2e^- \rightleftharpoons 2\text{-}HNQ^{3-};\quad E_0^{pH-14} = -0.501\ V\ vs\ SHE \quad (2)$$

$$O_2 + 2H_2O + 4e^- \rightleftharpoons 4OH^-;\quad E_0^{pH-14} = +0.401\ V\ vs\ SHE \quad (3)$$

where $E_0^{pH=14}$ (V vs the standard hydrogen electrode) is the formal redox potential of the redox reaction when the solution pH is 14. We note the term "2-HNQ" encompasses the neutral

https://doi.org/10.1021/acsomega.2c05798
ACS Omega 2022, 7, 40540−40547

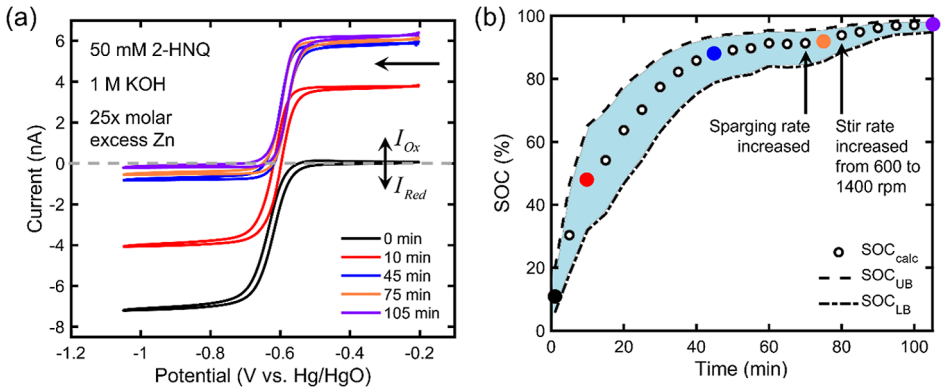

Figure 2. (a) Example microelectrode voltammograms from a representative data set where 2-HNQ is charged with Zn. The initial sweep direction is reductive (*via* the horizontal arrow); positive currents are oxidative, and negative currents are reductive. (b) Variation in the SOC at various times. $D_{Red}{\cdot}D_{Ox}^{-1}$ was assumed to be 1; the upper and lower bound estimates, $SOC_{UB/LB}$, respectively refer to $D_{Red}{\cdot}D_{Ox}^{-1} = 0.5$ and 2, with the range shaded in light blue. The filled circles correspond to the voltammograms in (a), and the sparging and stir rates were both increased to promote solution agitation.

powder, the dissociated oxidized form ("−1" charge), and the dissociated reduced form ("−3" charge). We also treat the two electron transfer processes as concerted for simplicity.[18] Further, eq 1 is the net result of zinc oxidation into zincate and its subsequent dissociation into zinc oxide, water, and hydroxyl species (*vide infra*) and, as such, does not have an assigned redox potential.[6]

$$2Zn + 8OH^- \rightleftharpoons 2Zn(OH)_4^{2-} + 4e^-; \quad E_0^{pH-14} = -1.199 \text{ V vs SHE} \tag{4}$$

$$2Zn(OH)_4^{2-} \rightleftharpoons 2ZnO + 2H_2O + 4OH^- \tag{5}$$

Equations 1, 4, and 5 are not fully reduced to demonstrate that the respective hydroxyl ion generation and consumption are balanced *via* the terminal products in the cathode and the anode (eqs 3 and 1, respectively), suggesting minimal pH swings during cell operation.

Estimating the Chemical Reduction of RMs Using Microelectrode Voltammetry. While the electrode reactions occurring within the flow cell (ORR and quinone oxidation) are reasonably well-understood,[16,19] the redox reactions between the RM and SEF have not been as extensively studied. As such, we sought to assess whether the selected metals can chemically reduce the solubilized RMs. We selected SEFs and RMs with sufficiently disparate electrode potentials to enable a suitable thermodynamic driving force—for example, Zn oxidizes at *ca.* −1.2 V versus SHE, and 2-HNQ has an observed redox potential of *ca.* −0.5 V versus SHE, resulting in a *ca.* 700 mV overpotential.

To measure the extent of the reaction, we used a three-electrode configuration to monitor the time-dependent changes in the RM state of charge (SOC) in the presence of a stoichiometric excess of SEF. Specifically, we used microelectrode voltammetry, where the small working electrode radius (*ca.* 1−10 μm) produces steady-state currents that simultaneously describe the charged and discharged active species concentrations, which, in turn, can be processed to estimate the solution SOC and state of health (SOH).[20−22]

Figure 2a shows representative microelectrode voltammograms acquired on a carbon fiber working electrode throughout the experiment, depicting changes in the steady-state current plateaus representative of the time-dependent SOC. To increase the rate of Zn/2-HNQ mixing and potentially the rate and extent of the chemical redox reaction at the upper limits of SOC, sparging was more aggressively conducted starting at 70 min; the stir rate, in turn, was increased from 600 to 1400 rpm at 80 min for the same purpose. Multiple independent trials ($n > 3$) were conducted; 2-HNQ was consistently reduced in these trials, supporting the data shown for the individual trial in Figure 2. We calculate the SOC (Figure 2b) by assuming a diffusion coefficient ratio of unity—$D_{Red}{\cdot}D_{Ox}^{-1} = 1$, where $D_{Red/Ox}$ ($m^2\ s^{-1}$) refers to the respective diffusion coefficients of the reduced and oxidized forms of a generic redox couple[23]—but we also consider differing ratios ($D_{Red}{\cdot}D_{Ox}^{-1} = 0.5$ and $D_{Red}{\cdot}D_{Ox}^{-1} = 2$) to respectively serve as upper and lower SOC bounds. This analysis enables a general trend to be discerned beyond the specific redox couples examined; we find that minor variations in this ratio do not significantly alter SOC predictions.

The Zn/2-HNQ electrolyte approaches *ca.* 97% SOC from an entirely discharged state (i.e., near-complete 2-HNQ reduction) within 2 h. Concurrently, the magnitude of the sigmoid wave (the apparent SOH) decreases by *ca.* 20%, which we suspect is largely due to a nonunity ($D_{Red}{\cdot}D_{Ox}^{-1} \sim 0.8$) diffusion coefficient ratio within the bounds of Figure 2b—rather than molecular decomposition—based on an overnight durability study of 2-HNQ examined in the Supporting Information and on literature precedent.[16,24] The other candidate RM−SEF pairs display significantly lower conversions over similar timescales, which we tentatively attribute to surface passivation. These semi-quantitative studies are intended to evaluate whether charge-transfer reactions occur between the RM and the SEF at appreciable rates; the development of microscopic rate laws and quantitative extensions to reactor-scale experiments and models require more comprehensive analyses beyond the scope of this initial report.

Estimating the Chemical Oxidation of SEFs *via* X-ray Diffraction and Optical Microscopy. While the prior experiments indicate that 2-HNQ is reduced in the presence of Zn, it is unclear whether Zn is the dominant electron source. As such, we performed a combination of X-ray diffraction and optical microscopy to explore the evolution of the Zn SEF in Figure 3.

Figure 3b depicts the baseline diffractogram (left column), optical micrograph (center column), and associated illustration

https://doi.org/10.1021/acsomega.2c05798
ACS Omega 2022, 7, 40540−40547

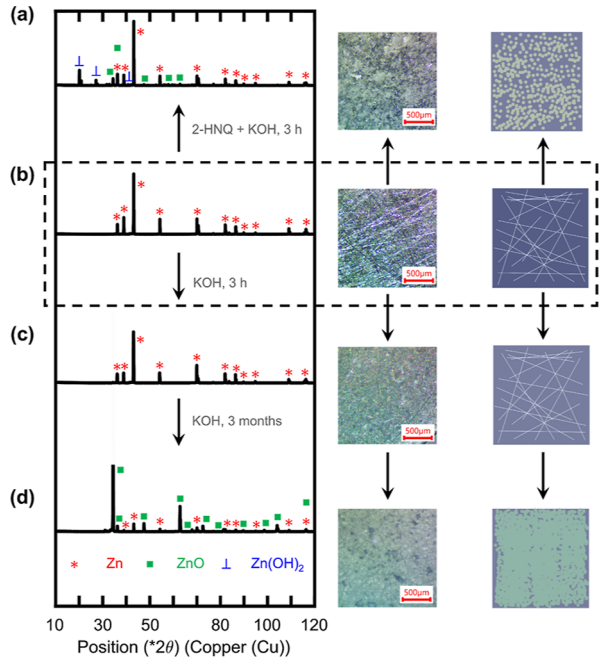

Figure 3. Diffractograms (left column), optical micrographs (center column), and illustrative diagrams (right column) of Zn-oxidation in 1 M potassium hydroxide (KOH) with and without 50 mM 2-HNQ. (a) Post mortem observations of Zn after residing in an aqueous solution of 50 mM 2-HNQ and 1 M KOH for 3 h. (b) Analogous observations for pristine, unreacted Zn. (c) Observations for Zn after residing in 1 M KOH (no 2-HNQ) for 3 h. (d) Observations for Zn after residing in 1 M KOH (no 2-HNQ) for 3 months. Vertically stacked symbols indicate that multiple species contributed to the observed diffractogram peak. In part (d), the larger ZnO peak near a 2θ of 35° was truncated to improve visibility. Within the illustrative diagrams, the dark and faded violet backgrounds respectively represent (un)tarnished Zn, the silver lines represent striations on the as-received Zn, and circles represent solid deposits. More detailed diffraction results are provided in the Supporting Information.

(right column) of Zn foil unexposed to the solution. Figure 3a indicates that ZnO and $Zn(OH)_2$ are present with the Zn after it resides in an aqueous solution of 50 mM 2-HNQ and 1 M KOH for 3 h. Figure 3c,d, in turn, indicates that though Zn oxidizes in a solution containing only water and 1 M KOH (no 2-HNQ), the reaction proceeds more slowly and possibly *via* different mechanisms—$Zn(OH)_2$ is not observed—suggesting Zn contributes toward reducing 2-HNQ. These findings generally agree with the current understanding of Zn-oxidation in alkaline conditions, which can proceed through multiple pathways.[6,25−28] A passivation layer may form but is thought to be porous,[29] allowing for a reduced, but finite, mass transfer of 2-HNQ to the buried Zn surface to continue the chemical redox reaction. The ZnO may form either on the surface of the Zn pellets or in the bulk solution, the latter of which could ultimately hamper performance due to clogging. Zinc composite blends (e.g., Zn, carbon black, and polyvinylidene fluoride), along with greater concentrations of KOH, may limit the potentially harmful homogeneous formation of ZnO and the precipitation of ZnO onto undesired surfaces (e.g., cell tubing).[7,8] Hydrogen evolution also generallly occurs as a product of Zn corrosion in alkaline solutions; though the presence of 2-HNQ (or any mediator) does not necessarily affect the rate of hydrogen evolution, in this specific system hydrogen evolution appears to be slower than 2-HNQ reduction, as evinced by Figure 3a,c. These analyses indicate that 2-HNQ is reduced in the electrolyte due primarily to its interactions with Zn, which is, in turn, corroded.

Proof-of-Concept Demonstration with a Hybrid Flow Cell Architecture. To explore the efficacy of the charge transfer between the SEF and RMs on a device level, proof-of-concept experiments were conducted with the 2-HNQ/Zn pairing using a flow cell architecture (Figure 4a) adopted from a prior design and modified to enable the ORR *via* a silver-coated gas diffusion electrode.[30] The same concentration of RM used in previous *ex situ* studies (50 mM) was deployed for consistency and to reduce the likelihood of undesired processes that can occur at higher organic analyte concentrations (e.g., oligomerization, ionic association);[31,32] future efforts can probe RM−SEF interactions at greater mediator concentrations (for 2-HNQ, up to 0.48 M[16]) to judiciously engineer SFFBs with greater power density. To ensure sufficient 2-HNQ charging from the Zn and adequate electrode wetting, we conduct open circuit voltage (OCV) studies, which should increase as the 2-HNQ charges according to the Nernst equation. Indeed, the OCV increases throughout the experiment; however, the maximum measured voltage (*ca.* 0.68 V) was lower than the theoretical (*ca.* 0.9 V) by *ca.* 200 mV. This is possibly due to reactant crossover causing mixed electrode potentials and/or catalyst poisoning.[33]

To demonstrate repeatable performance and to explore the behavior of the reactor at different discharge conditions, we assembled a second cell operated at various current densities up to *ca.* 10 mA cm^{-2}. With sufficient electrolyte flow (≥10 mL min^{-1}), the polarization behavior was largely insensitive to the O_2 flow rate (range 2−20 mL min^{-1}). Encouraged by these findings, we conducted a longer duration discharge experiment at an electrolyte flow rate of 10 mL min^{-1}, an O_2 flow rate of 2 mL min^{-1}, and a constant current density of 2 mA cm^{-2}, along with OCV measurements for 5 min every hour (not shown). Though not explored in this work, the current density may be readily increased by introducing greater concentrations of 2-HNQ, by leveraging a greater amount of zinc, and possibly by increasing the concentration of KOH; additional approaches (e.g., different cathode catalysts and improved membranes) will also result in greater current densities.

As shown in Figure 4b,c, the cell delivered an average voltage of *ca.* 0.38 V that gradually declined during the extended discharge period. During this time, the OCV similarly declined from 0.61 to 0.5 V, indicating that polarization was not the only factor limiting performance. We posit that the cause of this decay was material depletion *via* undesired water crossover to and evaporation from the cathode or other leak points in the testing apparatus. We also attribute the voltage fluctuations between 1.2 and 1.6 A h to flooding; in future iterations, greater oxygen back pressures—along with greater oxygen humidity—may decrease the rate of electrolyte loss through the cathode effluent stream.[34] 2-HNQ may also undergo chemical homogeneous or heterogeneous decomposition in the anodic half-cell—with the reduced mediator concentrations potentially leading to mass transport limitations that lower the cell voltage during operation—though we demonstrate in the Supporting Information that this decay mechanism is likely not the sole cause of performance degradation.[16,24] To allow the cell voltage to partially recover, the cell discharge was occasionally stopped for longer periods (>5 min)—referred to as "pauses"—and the electrolyte reservoir was sometimes refilled (respectively, denoted by the

https://doi.org/10.1021/acsomega.2c05798
ACS Omega 2022, 7, 40540−40547

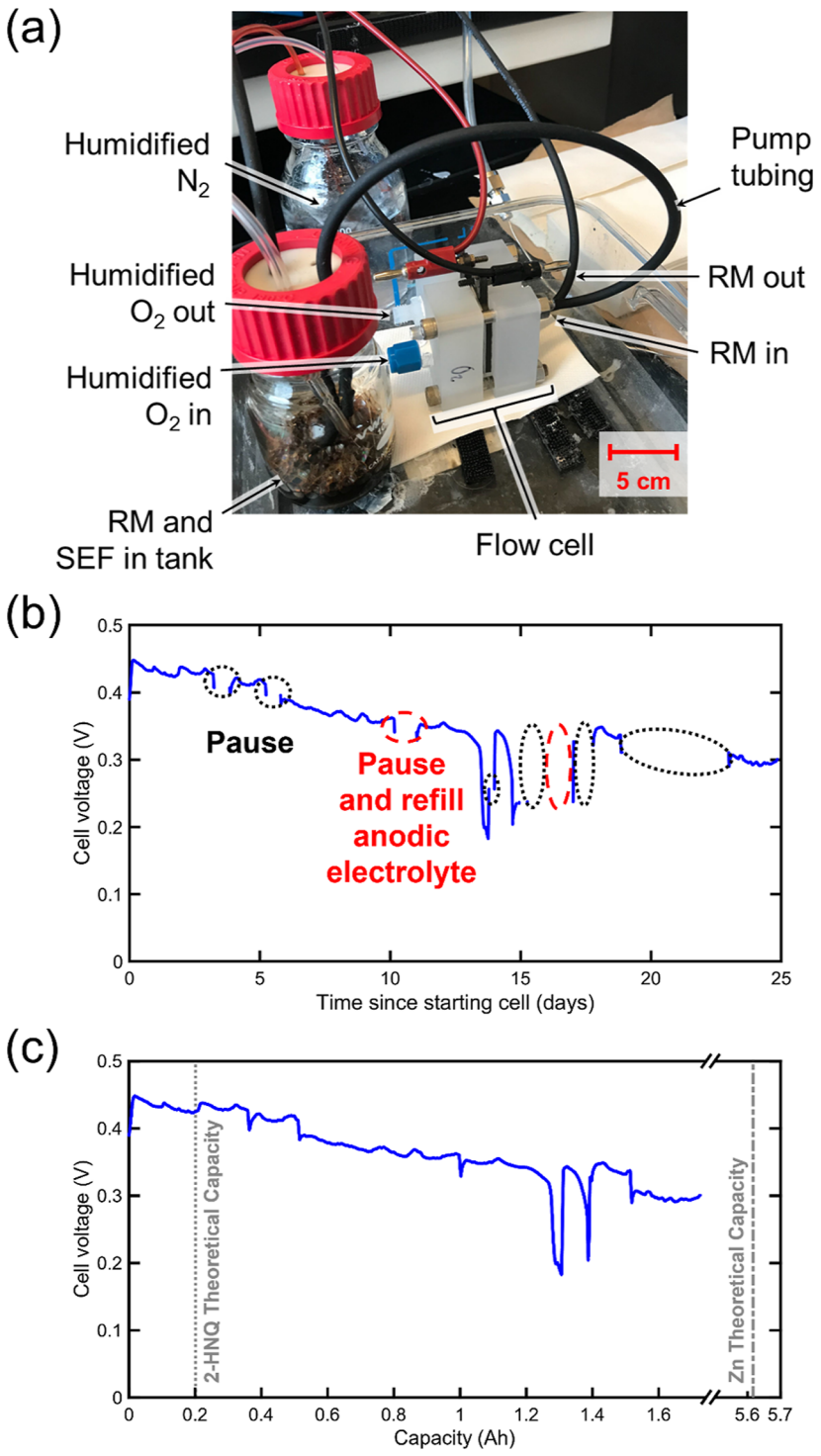

Figure 4. (a) Labeled photograph of the assembled SFFB used for OCV monitoring; the scale bar is qualitative. (b) Flow cell discharge, with outliers and smoothing processed using 1 h moving median and mean windows, respectively. Extended pauses in the galvanostatic discharge were taken (black or red circles), sometimes to refill the anodic electrolyte volume (red circles). (c) Same discharge curve as (b) plotted vs capacity.

black and red circles in Figure 4b); successful voltage recovery after pauses indicates that the tank reaction may be rate-limiting in this device. The longevity of the cell suggests that performance degradation was not rapid or could otherwise be mitigated; indeed, the experiment ended due to equipment needs rather than cell death. Overall, *ca.* 30% (1.725 A h) of the theoretical capacity (i.e., the overall Coulombic efficiency) from the Zn was accessed during *ca.* 25 days of galvanostatic discharge (Figure 4c). We anticipate that the Zn utilization may be greater if the cell had continued running; additional strategies (e.g., increased KOH concentrations and carbon–zinc slurries) may further extend the utilization of the SEF,[7,8] though material compatibility concerns (e.g., wetted components) may arise at more extreme pH values.

Like all metal–air batteries, the theoretical energy density is high, but the form factor and operating conditions dictate what

https://doi.org/10.1021/acsomega.2c05798
ACS Omega 2022, 7, 40540–40547

is practically achievable. This prototype has a low energy density (5 W h L^{-1}), but this is largely due to the device construction (e.g., the 250 mL storage tank). The voltaic efficiency—the average cell voltage normalized by the OCV—is also low at 23% when referencing zinc oxidation and the ORR (OCV = 1.6 V), though this value increases to 41% when using the OCV between 2-HNQ oxidation and the ORR (0.902 V). That said, improvements in cell design and engineering are expected to reduce the gap between the theoretical and achievable cell voltages.

CONCLUSIONS

In this study, we explore an energy storage concept—an SFFB—that seeks to combine the high energy density of a metal−air battery with the architecture of an RFB. Using a combination of electrochemical, X-ray diffraction, and optical microscopy methods, we identified 2-HNQ and Zn as a promising material set. Finally, we demonstrated the feasibility of this approach using a proof-of-concept flow cell setup which operated for *ca.* 25 days, accessing *ca.* 30% of the theoretical capacity of the Zn in the reservoir.

While these exploratory studies suggest that the SFFB may hold promise as a modular and energy-dense device, further studies are needed both to understand the potential of this storage approach and to improve its performance. Microscopic analyses of the rates and selectivity of the charge-transfer reactions between the soluble mediator and solid fuel are needed to articulate reaction rate laws. These studies would further identify opportunities to enhance performance, accessible capacity, and longevity through material selection and electrolyte engineering. Of particular importance are the roles of thermodynamic driving force and evolving interfacial chemistry on observed reaction rates. Further, refinements in membrane-electrode assembly engineering may enable improvements in operating cell potential and current density through reductions in cell resistance, increases in catalytic/electrode activity, and mitigation of mediator crossover and water evaporation. Finally, system design and engineering efforts are needed to correctly size the tank and electrochemical reactor to maximize the overall performance.

EXPERIMENTAL METHODS

Materials and Reagents. 2-HNQ (Thermo Scientific, AAA1188009, 98+%) and KOH (Sigma-Aldrich, P1767, ≥85%) were used as received. Zn foil of 0.25 mm thickness (Thermo Scientific, AA10436BW, 99.98%) was hand cut with shears into smaller pieces (each *ca.* 1−5 cm^2) before being added to the solution containing the RM. Details on other RM−SEF pairings are provided in the Supporting Information.

Microelectrode Experiments. The electrolyte solutions tested consisted of 50 mM 2-HNQ and 1 M KOH dissolved in deionized water (18.2 MΩ cm) equipped with a carbon fiber microelectrode (Bioanalytical Systems, Inc. (BASi), MF-2007, 8−13 μm nominal diameter range); a platinum(Pt) coil (BASi, MW-1033), wire (BASi, MW-1032), or mesh counter electrode; and a Hg/HgO reference electrode (BASi, EF-1369). Polishing was conducted using 0.05 μm alumina powder (Buehler, MicroPolish Powder, 4010075) in deionized water. To remove residual O_2, the system was initially sparged for 10 min with N_2 (Airgas, 99.999%) humidified in-house. An initial (set of) voltammogram(s) was acquired before the addition of the Zn, after which 25 molar equivalents (*ca.* 0.82 g) of the Zn foil were added to chemically reduce 2-HNQ. We then recorded microelectrode voltammograms at various time intervals—typically 5 min—to monitor the RM SOC at room temperature (20−25 °C). A stir bar (VWR, 58948-375) was also used to promote mixing; during voltammetric acquisition, the stir bar was stopped, and the sparging line was raised above the electrolyte, to enable solution quiescence. To increase the chemical redox reaction rate, both the rate of sparging and stirring were occasionally increased.

X-ray Diffractometry Experiments. X-ray diffractograms of Zn were acquired using a PANalytical X'Pert PRO XRPD (1.8 kW sealed X-ray tube source with a copper target and a vertical circle theta/theta goniometer, 240 mm radius). PANalytical HighScore Plus was used to regress the constituent phases from the diffractograms to a library referenced from the International Center for Diffraction Data PDF database.

Optical Microscopy Experiments. Optical microscopy was performed on a 7−45× magnification industrial inspection microscope (AmScope) equipped with a 9.0 MP USB camera and 20×/10 eyepieces (AmScope). Software provided by AmScope was used for image acquisition, with the scale calibrated with an external optical reference micrometer scale. LED top-down illumination was used for opaque metal samples, and focusing was manually adjusted for each magnification level. Samples were imaged as extracted after experiments, subsequently rinsed in DI water for 30 s, and imaged again. All expended metal samples were stored in high-density polyethylene scintillation vials (VWR).

Full Cell Studies. Two separate cells were studied for repeatability—one for an OCV analysis and another for polarization and long-term operation studies. Major components included graphite interdigitated flow fields, porous electrodes, an anion-exchange membrane (Membranes International Inc., AMI-7001S), and plastic backing plates. The anode was a carbon paper electrode (Sigracet 29AA) thermally treated in air at 400 °C for 30 h to improve aqueous electrolyte wetting. The cathode was a hydrophobically treated carbon paper gas diffusion electrode (Freudenberg H23C6, Fuel Cell Store) with a silver (Ag)-nanoparticle-based catalyst layer spray coated onto the microporous layer; the catalyst-coated side of the cathode was abutted to the membrane to enable the ionic connection. Both electrodes were compressed to *ca.* 75% of their nominal thickness to provide sufficient conductivity and reduce contact resistances.

Further, a Masterflex peristaltic pump (Cole Parmer) with Masterflex Norprene tubing (size: L/S 14, Cole Parmer) was used to circulate the electrolyte. The electrolyte flowed through the anodic half cell at various flow rates, and high purity O_2 (Airgas, OX UHP300) was passed through the cathode. The setup also included the gas flow controllers (Brooks Instruments) and an in-house gas humidification unit to, respectively, control the O_2 flow rate and humidify the inlet gas at ambient temperature; the humidity level was not quantified throughout the experiment but is estimated to be *ca.* 20 wt % based on thermodynamic calculations. An NPT-type fitting was used to connect the oxygen line to the reactor. For the anodic side, the storage tank on the anode side was a 100 mL (for the first cell) or 250 mL (for the second cell) glass media bottle which contained the aqueous electrolyte (50 mM 2-HNQ dissolved in 1 M KOH) and, initially, *ca.* 1.8 g of the hand-cut Zn foil. The tank was sealed using a rubber septum with four holes punched—two 3/16″ holes for the electrolyte

https://doi.org/10.1021/acsomega.2c05798
ACS Omega 2022, 7, 40540−40547

inlet/outlet, one 3/16″ hole for the sparging line (N_2 humidified in-house), and one uncovered 1/8″ or 3/16″ hole to prevent overpressure.

All cells were operated at room temperature (20−25 °C). The OCV of the first cell that contained 20 mL of electrolyte in the storage tank was monitored for *ca.* 12 h. The subsequent cell, in turn, contained 75 mL of electrolyte and was operated at various current densities up to *ca.* 10 mA cm^{-2}. This second cell was also operated for a long-duration study at an electrolyte flow rate of 10 mL min^{-1}, an O_2 flow rate of 2 mL·min^{-1}, and a constant current density of 2 mA cm^{-2}; the OCV was also measured for 5 min every hour. Extra Zn (prepared as before) was also added for the long-duration cycling to replicate the same stoichiometric excess used in the microelectrode studies—*ca.* 25×, or 6.85 g (5.617 A h capacity), in total.

■ ASSOCIATED CONTENT

Supporting Information

The Supporting Information is available free of charge at https://pubs.acs.org/doi/10.1021/acsomega.2c05798.

Additional details regarding microelectrode voltammetry theory and experiments; molecular stability of 2-HNQ; results and experimental details for all four material pairings, with microelectrode voltammetry analyses for the 2,6-DHAQ/Zn, 2,6-DHAQ/Fe, and 2-HNQ/Fe pairings; description of cell assembly and catalyst preparation/spray-coating; full cell results for OCV and polarization tests; and raw X-ray diffractograms and tabulated peaks (PDF)

■ AUTHOR INFORMATION

Corresponding Author

Fikile R. Brushett − *Department of Chemical Engineering, Massachusetts Institute of Technology, Cambridge, Massachusetts 02139, United States;* orcid.org/0000-0002-7361-6637; Phone: +16173247400; Email: brushett@mit.edu

Authors

Alexis M. Fenton, Jr. − *Department of Chemical Engineering, Massachusetts Institute of Technology, Cambridge, Massachusetts 02139, United States;* orcid.org/0000-0003-2195-9408

Yasser Ashraf Gandomi − *Department of Chemical Engineering, Massachusetts Institute of Technology, Cambridge, Massachusetts 02139, United States;* orcid.org/0000-0003-2546-1754

Christopher T. Mallia − *Department of Materials Science and Engineering, Massachusetts Institute of Technology, Cambridge, Massachusetts 02139, United States*

Bertrand J. Neyhouse − *Department of Chemical Engineering, Massachusetts Institute of Technology, Cambridge, Massachusetts 02139, United States;* orcid.org/0000-0001-6747-8197

M. Aba Kpeglo − *Department of Chemical Engineering, Massachusetts Institute of Technology, Cambridge, Massachusetts 02139, United States*

William E. Exson − *Department of Chemical Engineering, Massachusetts Institute of Technology, Cambridge, Massachusetts 02139, United States*

Charles Tai-Chieh Wan − *Department of Chemical Engineering, Massachusetts Institute of Technology, Cambridge, Massachusetts 02139, United States;* orcid.org/0000-0002-9324-202X

Complete contact information is available at: https://pubs.acs.org/10.1021/acsomega.2c05798

Author Contributions

¶A.M.F., Jr. and Y.A.G. equal lead author contribution. A.M.F., Jr. performed the conceptualization, methodology, software, validation, formal analysis, investigation, data curation, writing—original draft, writing—review and editing, and visualization. Y.A.G. performed the conceptualization, methodology, software, validation, formal analysis, investigation, data curation, writing—original draft, writing—review and editing, and visualization. C.T.M. performed the validation, investigation, data curation, writing—original draft, writing—review and editing, and visualization. B.J.N. performed the writing—original draft, writing—review and editing, and visualization. M.A.K. performed the validation, investigation, and writing—review and editing. W.E.E. performed the validation, investigation, and writing—review and editing. C.T.W. performed the methodology, validation, investigation, writing—review and editing, and visualization. F.R.B. performed the conceptualization, funding acquisition, project administration, resources, supervision, writing—original draft, writing—review and editing.

Notes

The authors declare no competing financial interest.

■ ACKNOWLEDGMENTS

This work was funded by the Skoltech—MIT Next Generation Program. Y.A.G., B.J.N., C.T.W., and F.R.B. gratefully acknowledge support from the Joint Center for Energy Storage Research, an Energy Innovation Hub funded by the U.S. Department of Energy, Office of Science, Basic Energy Sciences. B.J.N. and C.T.W. gratefully acknowledge the NSF Graduate Research Fellowship Program under grant numbers 2141064 (B.J.N.) and 1745302 (C.T.W.). Any opinion, findings, conclusions, or recommendations expressed in this material are those of the authors and do not necessarily reflect the views of the NSF. C.T.M. gratefully acknowledges support under and awarded by the Department of Defense, Office of Naval Research, through the National Defense Science and Engineering Graduate Fellowship. The authors thank MIT's Undergraduate Research Opportunity Program for funding support.

■ REFERENCES

(1) Huang, Q.; Li, H.; Grätzel, M.; Wang, Q. Reversible chemical delithiation/lithiation of LiFePO4: towards a redox flow lithium-ion battery. *Phys. Chem. Chem. Phys.* **2013**, *15*, 1793−1797.

(2) Weber, A. Z.; Mench, M. M.; Meyers, J. P.; Ross, P. N.; Gostick, J. T.; Liu, Q. Redox Flow Batteries: A Review. *J. Appl. Electrochem.* **2011**, *41*, 1137−1164.

(3) Rahman, Md. A.; Wang, X.; Wen, C. High Energy Density Metal-Air Batteries: A Review. *J. Electrochem. Soc.* **2013**, *160*, A1759−A1771.

(4) Mladenova, E.; Slavova, M.; Mihaylova-Dimitrova, E.; Burdin, B.; Abrashev, B.; Krapchanska, M.; Raikova, G.; Vladikova, D. Monolithic Carbon-Free Gas Diffusion Electrodes for Secondary Metal-Air Batteries. *J. Electroanal. Chem.* **2021**, *887*, 115112.

(5) Blurton, K. F.; Sammells, A. F. Metal/air batteries: Their status and potential - a review. *J. Power Sources* **1979**, *4*, 263−279.
(6) Li, Y.; Dai, H. Recent Advances in Zinc-Air Batteries. *Chem. Soc. Rev.* **2014**, *43*, 5257−5275.
(7) Perez-Antolin, D.; Schuhmann, W.; Palma, J.; Ventosa, E. Semi-Flowable Zn Semi-Solid Electrodes as Renewable Energy Carrier for Refillable Zn−Air Batteries. *J. Power Sources* **2022**, *536*, 231480.
(8) Zhang, H.; Huang, S.; Salla, M.; Zhuang, J.; Gao, M.; Lek, D. G.; Ye, H.; Wang, Q. A Redox-Mediated Zinc−Air Fuel Cell. *ACS Energy Lett.* **2022**, *7*, 2565−2575.
(9) Wang, Q.; Zakeeruddin, S. M.; Wang, D.; Exnar, I.; Grätzel, M. Redox Targeting of Insulating Electrode Materials: A New Approach to High-Energy-Density Batteries. *Angew. Chem., Int. Ed.* **2006**, *45*, 8197−8200.
(10) Huang, Q.; Yang, J.; Ng, C. B.; Jia, C.; Wang, Q. A Redox Flow Lithium Battery Based on the Redox Targeting Reactions between $LiFePO_4$ and Iodide. *Energy Environ. Sci.* **2016**, *9*, 917−921.
(11) Yang, L.; Liu, W.; Zhang, Z.; Du, X.; Gong, J.; Dong, L.; Deng, Y. Hydrogen Evolution from Native Biomass with Fe^{3+}/Fe^{2+} Redox Couple Catalyzed Electrolysis. *Electrochim. Acta* **2017**, *246*, 1163−1173.
(12) Anson, C. W.; Stahl, S. S. Mediated Fuel Cells: Soluble Redox Mediators and Their Applications to Electrochemical Reduction of O_2 and Oxidation of H_2, Alcohols, Biomass, and Complex Fuels. *Chem. Rev.* **2020**, *120*, 3749−3786.
(13) Moghaddam, M.; Sepp, S.; Wiberg, C.; Bertei, A.; Rucci, A.; Peljo, P. Thermodynamics, Charge Transfer and Practical Considerations of Solid Boosters in Redox Flow Batteries. *Molecules* **2021**, *26*, 2111.
(14) Zhang, F.; Gao, M.; Huang, S.; Zhang, H.; Wang, X.; Liu, L.; Han, M.; Wang, Q. Redox Targeting of Energy Materials for Energy Storage and Conversion. *Adv. Mater.* **2022**, *34*, 2104562.
(15) McKerracher, R. D.; Ponce de Leon, C.; Wills, R. G. A.; Shah, A. A.; Walsh, F. C. A Review of the Iron-Air Secondary Battery for Energy Storage. *ChemPlusChem* **2015**, *80*, 323−335.
(16) Tong, L.; Goulet, M.-A.; Tabor, D. P.; Kerr, E. F.; De Porcellinis, D. D.; Fell, E. M.; Aspuru-Guzik, A.; Gordon, R. G.; Aziz, M. J. Molecular Engineering of an Alkaline Naphthoquinone Flow Battery. *ACS Energy Lett.* **2019**, *4*, 1880−1887.
(17) Lin, K.; Chen, Q.; Gerhardt, M. R.; Tong, L.; Kim, S. B.; Eisenach, L.; Valle, A. W.; Hardee, D.; Gordon, R. G.; Aziz, M. J.; Marshak, M. P. Alkaline Quinone Flow Battery. *Science* **2015**, *349*, 1529−1532.
(18) Quan, M.; Sanchez, D.; Wasylkiw, M. F.; Smith, D. K. Voltammetry of Quinones in Unbuffered Aqueous Solution: Reassessing the Roles of Proton Transfer and Hydrogen Bonding in the Aqueous Electrochemistry of Quinones. *J. Am. Chem. Soc.* **2007**, *129*, 12847−12856.
(19) Hayre, R. O'.; Cha, S.-W.; Colella, W.; Prinz, F. B.Chapter 8: Overview of Fuel Cell Types. *Fuel Cell Fundamentals*; John Wiley & Sons, Inc.: Hoboken, 2016; pp 272−302.
(20) Stolze, C.; Meurer, J. P.; Hager, M. D.; Schubert, U. S. An Amperometric, Temperature-Independent, and Calibration-Free Method for the Real-Time State-of-Charge Monitoring of Redox Flow Battery Electrolytes. *Chem. Mater.* **2019**, *31*, 5363−5369.
(21) Kowalski, J. A.; Fenton, A. M., Jr.; Neyhouse, B. J.; Brushett, F. R. A Method for Evaluating Soluble Redox Couple Stability Using Microelectrode Voltammetry. *J. Electrochem. Soc.* **2020**, *167*, 160513.
(22) Neyhouse, B. J.; Tenny, K. M.; Chiang, Y.-M.; Brushett, F. R. Microelectrode-Based Sensor for Measuring Operando Active Species Concentrations in Redox Flow Cells. *ACS Appl. Energy Mater.* **2021**, *4*, 13830−13840.
(23) Compton, R. G.; Banks, C. E.*Understanding Voltammetry*, 2nd ed.; Imperial College Press: London, 2011.
(24) Wang, C.; Yang, Z.; Wang, Y.; Zhao, P.; Yan, W.; Zhu, G.; Ma, L.; Yu, B.; Wang, L.; Li, G.; Liu, J.; Jin, Z. High-Performance Alkaline Organic Redox Flow Batteries Based on 2-Hydroxy-3-Carboxy-1,4-Naphthoquinone. *ACS Energy Lett.* **2018**, *3*, 2404−2409.
(25) Nichols, J. T.; McLarnon, F. R.; Cairns, E. J. Zinc Electrode Cycle-Life Performance in Alkaline Electrolytes Having Reduced Zinc Species Solubility. *Chem. Eng. Commun.* **1985**, *37*, 355−379.
(26) Thomas, S.; Cole, I. S.; Sridhar, M.; Birbilis, N. Revisiting Zinc Passivation in Alkaline Solutions. *Electrochim. Acta* **2013**, *97*, 192−201.
(27) Ko, Y.; Park, S.-M. Zinc Oxidation in Dilute Alkaline Solutions Studied by Real-Time Electrochemical Impedance Spectroscopy. *J. Phys. Chem. C* **2012**, *116*, 7260−7268.
(28) *CRC Handbook of Chemistry and Physics*, 102nd ed.; Rumble, J. R.; CRC Press: Boca Raton, 2021.
(29) Stamm, J.; Varzi, A.; Latz, A.; Horstmann, B. Modeling Nucleation and Growth of Zinc Oxide during Discharge of Primary Zinc-Air Batteries. *J. Power Sources* **2017**, *360*, 136−149.
(30) Milshtein, J. D.; Barton, J. L.; Darling, R. M.; Brushett, F. R. 4-Acetamido-2,2,6,6-Tetramethylpiperidine-1-Oxyl as a Model Organic Redox Active Compound for Nonaqueous Flow Batteries. *J. Power Sources* **2016**, *327*, 151−159.
(31) Zhao, E. W.; Jónsson, E.; Jethwa, R. B.; Hey, D.; Lyu, D.; Brookfield, A.; Klusener, P. A. A.; Collison, D.; Grey, C. P. Coupled In Situ NMR and EPR Studies Reveal the Electron Transfer Rate and Electrolyte Decomposition in Redox Flow Batteries. *J. Am. Chem. Soc.* **2021**, *143*, 1885−1895.
(32) Shkrob, I. A.; Robertson, L. A.; Yu, Z.; Assary, R. S.; Cheng, L.; Zhang, L.; Sarnello, E.; Liu, X.; Li, T.; Preet Kaur, A. P.; Malsha Suduwella, T. M.; Odom, S. A.; Wang, Y.; Ewoldt, R. H.; Farag, H. M.; Z, Y. Crowded Electrolytes Containing Redoxmers in Different States of Charge: Solution Structure, Properties, and Fundamental Limits on Energy Density. *J. Mol. Liq.* **2021**, *334*, 116533.
(33) Lei, C.; Yang, F.; Macauley, N.; Spinetta, M.; Purdy, G.; Jankovic, J.; Cullen, D. A.; More, K. L.; Kim, Y. S.; Xu, H. Impact of Catalyst Ink Dispersing Solvent on PEM Fuel Cell Performance and Durability. *J. Electrochem. Soc.* **2021**, *168*, 044517.
(34) Kimball, E.; Whitaker, T.; Kevrekidis, Y. G.; Benziger, J. B. Drops, Slugs, and Flooding in Polymer Electrolyte Membrane Fuel Cells. *AIChE J.* **2008**, *54*, 1313−1332.

https://doi.org/10.1021/acsomega.2c05798
ACS Omega 2022, 7, 40540−40547